Chin. J. Chem. Eng., **15**(4) 478—485 (2007)

Modelling and Experimental Investigation of Humidification-Dehumidification Desalination Using a Carbon-Filled-Plastic Shell-Tube Column*

CHENG Huaigang(成怀刚) **and WANG Shichang**(王世昌)**
Chemical Engineering Research Center, State Key Laboratory of Chemical Engineering, School of Chemical Engineering and Technology, Tianjin University, Tianjin 300072, China

Abstract The modelling and experimental investigation of a thermally coupled humidification-dehumidification desalination process using a carbon-filled-polypropylene shell-tube column are presented. A heat/mass transfer model is established to study the correlation among productivity, thermal efficiency, physicochemical parameters (gas/liquid phase temperature, heat/mass transfer coefficient, Reynolds number *etc*.), and operating conditions (the temperature of feed water, the flow rates of external steam, feed water, and carrier air); at the same time, the effects of operating conditions on the productivity and thermal eficiency of the column are investigated both theoretically and experimentally, which indicate that the optimum flow rates of external steam, feed water, and carrier gas are 0.18, 60, and 10kg·h^{-1}, respectively, and the higher the feed water temperature (≤95℃) is, the greater the productivity and the thermal efficiency will be. Furthermore, performance comparison with the previous study shows that the condensate productivity of this carbon-filled-plastic column is not lower than that of the copper column, which demonstrates the practicability and feasibility of applying such a plastic column to the humidification-dehumidification desalination process.
Keywords desalination, humidification-dehumidification, carbon-filled-polypropylene, simulation

1 INTRODUCTION

Industrial desalination of sea and brackish water is becoming more and more important in the water supply around the world. The common desalination techniques, such as multi-stage flash distillation (MSF), multi-effect distillation (MED), and reverse osmosis (RO), are not easy to operate and maintain, and thus economically competitive only for production on a large-scale (thousands of m^3·d^{-1})[1]. For this reason, these techniques are not suitable for water-shortage areas where potable water demand is decentralized, such as in the numerous small islands and remote northwest regions of China. So it will be very meaningful for these places to develop economically sustainable desalination methods, especially those using the local renewable or recovered energy. One of the most promising methods is desalination by humidification and dehumidification (HD) of air, the advantages of which include flexibility in capacity, moderate installation and operating costs, simplicity, and possibility of using low-grade thermal energy (solar, geothermal and waste heat *etc*.)[2, 3].

Many researches[4—10] have focused on the HD process using two separate units, one for humidification and another for dehumidification, where the vapor evaporated from the saline feed is carried by the gas-flow from the humidification unit to the dehumidification unit, and then condensates back to water again. In the humidification unit, the latent heat for vaporization mainly comes from the sensible heat of feed water or carrier gas. Meanwhile, the condensation latent heat in the dehumidification unit is nearly lost or partially reused to preheat feed water, in which process the thermal efficiency is low because of the large temperature difference. In 1988, Albers and Beckman[11] proposed a thermally coupled HD process known as dew vaporation, which combined the humidification and dehumidification processes by means of directly introducing condensation latent heat from the dehumidification unit to the humidification unit and enhancing the evaporation of saline water. Beckman *et al*., developed several dew vaporation towers with flat frame configuration, using REXAM, polypropylene (PP), and extruded PP twin wall sheets, respectively[12—14]. Xiong *et al*.[15] set up another copper HD column with shell-tube configuration, which could make the equipment simpler and more compact, and more efficient in the utilization of heat transfer area.

On the basis of Xiong's study, another pilot device is developed, in which the heat transfer tubes are made from novel carbon-filled polypropylene (CFP)[16]. Such a material is technologically suitable, inexpensive, rigid, light weight, easy to clean, scale-resistant, corrosion-resistant, aggressive-media-resistant, and of high thermal conductivity, which could potentially lead to extensive application in the HD desalination process. As far as in known literature, the applications of CFP in the thermally coupled HD process are not yet available. The objective of this work is to study both theoretically and experimentally the effects of operating conditions (flow rates of external steam, feed water and carrier gas, temperature of feed water) on the actual performance of this HD process using the CFP shell-tube column.

Received 2006-06-07, accepted 2007-04-28.
* Supported by the National Natural Science Foundation of China and China Energy Conservation Investment Corporation as a Key Project (No.20236030).
** To whom correspondence should be addressed. E-mail: jiswang@tju.edu.cn

2 EXPERIMENTAL MODULE AND MATHEMATICAL MODEL

The principle of thermally coupled HD process is shown in Fig.1. The humidification and dehumidification process are simultaneously performed at the tube and shell side of the column respectively. Initially, the preheated feed water flows down along the inner surfaces of the vertical tubes and vaporizes to vapor; meanwhile, low temperature, but saturated carrier gas (air) is also brought into the tube side from the tube bottom and moves upwards, mixing with the vapor and rising in temperature. Following this, at the top of the column some external steam at atmospheric pressure is added into the humid air to further increase its temperature and enthalpy a little; and then the hotter humid air is introduced into the shell-side and condensed on the outer surfaces of the tubes; the condensation latent heat is conducted to the tube-side liquid film, which would enhance the evaporation of the saline water. Finally, the air and the product (condensate water) leave the column from the lower outlet.

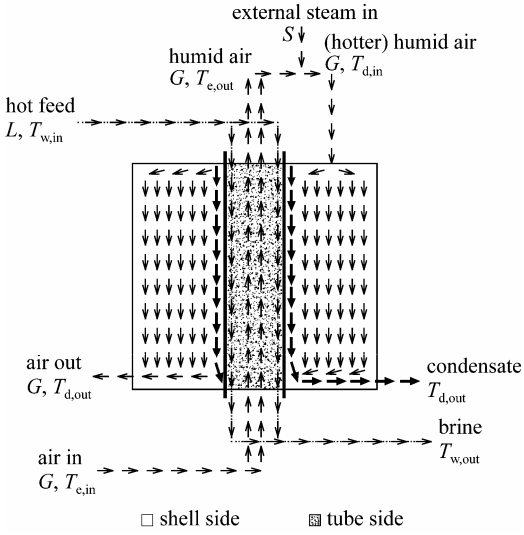

Figure 1 Sketch of HD column

As shown in Fig.2, a semi-experimental model[17] has been established. In that model, the heat and mass transfer coefficients are correlated from the experimental data of the copper column, so its application to the plastic column is limited. As for this study, the coefficient equations from the literature, which are not dependent on the given equipment configuration, are imported to update the model and analyze the experimental results.

2.1 Basic mathematical model

The following assumptions are considered when establishing the model:

(1) The water heat capacity, C_p, is constant.

(2) The temperature of the tube equates to that of the tube-side liquid film at the same location.

(3) Humidity of the air at the top and bottom of the column are measured and found saturated. In this model, it is assumed that the air is always saturated during the whole process.

As shown in Fig.2, the heat/mass transfer model of the HD process is constructed by extracting a differential unit from the column in Fig.1, and the mathematical descriptions (equations for heat/mass balance and transfer rates) are given as:

$$\mathrm{d}\left(G\cdot W_\mathrm{e}\right)=\mathrm{d}\left(L\cdot C_p\cdot T_\mathrm{w}\right)+\mathrm{d}Q \tag{1}$$

$$\mathrm{d}\left(G\cdot W_\mathrm{d}\right)+\mathrm{d}\left(F\cdot C_p\cdot T_\mathrm{d}\right)=\mathrm{d}Q+\mathrm{d}Q_\mathrm{Loss} \tag{2}$$

$$\mathrm{d}L=G\cdot\mathrm{d}H_\mathrm{e} \tag{3}$$

$$\mathrm{d}F=-G\cdot\mathrm{d}H_\mathrm{d} \tag{4}$$

$$G\cdot\mathrm{d}H_\mathrm{e}=k_H\cdot\left(H_\mathrm{w}-H_\mathrm{e}\right)\cdot\mathrm{d}A_H \tag{5}$$

$$\mathrm{d}Q=K\cdot\left(T_\mathrm{d}-T_\mathrm{w}\right)\cdot\mathrm{d}A \tag{6}$$

$$\mathrm{d}Q_\mathrm{Loss}=K_\mathrm{Loss}\cdot\left(T_\mathrm{d}-T_\mathrm{amb}\right)\cdot\mathrm{d}A_\mathrm{Loss} \tag{7}$$

All the variables, *Q*, *G*, *L*, *etc*., will be further specified in the nomenclature. These above equations can be rearranged to obtain[17]:

$$\frac{\mathrm{d}T_\mathrm{d}}{\mathrm{d}Z}=\frac{K\cdot n_1\cdot\left(T_\mathrm{d}-T_\mathrm{w}\right)+K_\mathrm{Loss}\cdot n_3\cdot\left(T_\mathrm{d}-T_\mathrm{amb}\right)}{G\cdot m_2+F\cdot C_p-G\cdot m_4\cdot C_p\cdot T_\mathrm{d}} \tag{8}$$

$$\frac{\mathrm{d}T_\mathrm{e}}{\mathrm{d}Z}=\frac{k_H\cdot n_2\cdot\left(H_\mathrm{w}-H_\mathrm{e}\right)}{G\cdot m_3} \tag{9}$$

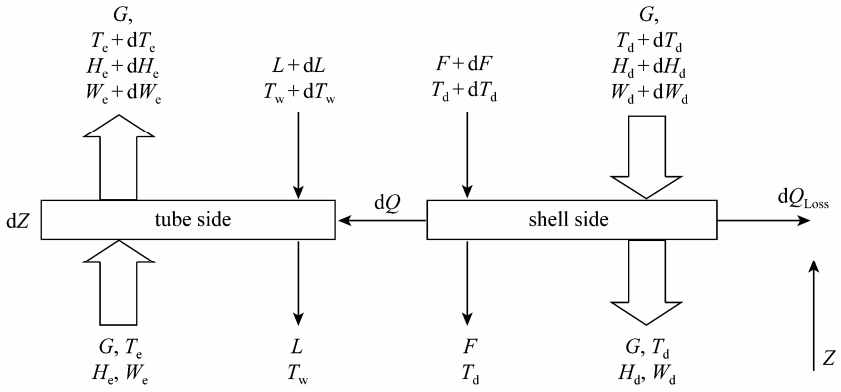

Figure 2 Schematic heat-mass transfer model of HD process

$$\frac{\mathrm{d}T_\mathrm{w}}{\mathrm{d}Z}=\left[k_H\cdot n_2\cdot\left(m_1-m_3\cdot C_p\cdot T_\mathrm{w}\right)\cdot\left(H_\mathrm{w}-H_\mathrm{e}\right)-m_3\cdot K\cdot n_1\cdot\left(T_\mathrm{d}-T_\mathrm{w}\right)\right]\Big/ m_3\cdot L\cdot C_p \tag{10}$$

$$\frac{\mathrm{d}L}{\mathrm{d}Z}=k_H\cdot n_2\cdot\left(H_\mathrm{w}-H_\mathrm{e}\right) \tag{11}$$

$$\frac{\mathrm{d}F}{\mathrm{d}Z}=\left\{-G\cdot m_4\times\left[K\cdot n_1\cdot\left(T_\mathrm{d}-T_\mathrm{w}\right)+K_\mathrm{Loss}\cdot n_3\cdot\left(T_\mathrm{d}-T_\mathrm{amb}\right)\right]\right\}\Big/\left(G\cdot m_2+F\cdot C_p-G\cdot m_4\cdot C_p\cdot T_\mathrm{d}\right) \tag{12}$$

where m represents the intermediate variable in the model. $m_1=\mathrm{d}W_\mathrm{e}/\mathrm{d}T_\mathrm{e}$, $m_2=\mathrm{d}W_\mathrm{d}/\mathrm{d}T_\mathrm{d}$, $m_3=\mathrm{d}H_\mathrm{e}/\mathrm{d}T_\mathrm{e}$ and $m_4=\mathrm{d}H_\mathrm{d}/\mathrm{d}T_\mathrm{d}$, all of which can be calculated from the thermodynamic property data of humid air[18]. n is the structural parameter. $n_1=\mathrm{d}A/\mathrm{d}Z=A/Z$, $n_2=\mathrm{d}A_H/\mathrm{d}Z=A_H/Z$ and $n_3=\mathrm{d}A_\mathrm{Loss}/\mathrm{d}Z=A_\mathrm{Loss}/Z$.

2.2 Mass transfer coefficient

In the above equations, k_H is the tube-side mass transfer coefficient based on the difference of humidity $\left(H_\mathrm{w}-H_\mathrm{e}\right)$.

$$k_H=k_c\frac{M_\mathrm{A}}{M_\mathrm{A}/\rho_\mathrm{dry\text{-}air}}=k_c\cdot\rho_\mathrm{dry\text{-}air} \tag{13}$$

where k_c is the gas phase mass transfer coefficient based on the difference of molar vapor concentration in the tube-side air between the liquid-gas (water-air) interface and the bulk gas (air). k_c is defined by Eq.(14) on the condition of laminar gas flow, and Eq.(15) on the condition of turbulent flow, respectively[19].

$$k_c=Sh\frac{D_\mathrm{AB}}{d}\frac{P}{p_\mathrm{BM}}=\left[3.66+\frac{0.0668\left(\dfrac{\mathrm{d}}{\mathrm{d}Z}ReSc\right)}{1+0.04\left(\dfrac{\mathrm{d}}{\mathrm{d}Z}ReSc\right)^{2/3}}\right]\frac{D_\mathrm{AB}}{d}\frac{P}{p_\mathrm{BM}} \tag{14}$$

$$k_c=0.023\times\frac{PD_\mathrm{AB}}{p_\mathrm{BM}d}Re^{0.83}Sc^{1/3} \tag{15}$$

p_BM is the air partial pressure difference between the liquid-gas interface and the bulk gas, and the saturated vapor pressure at the liquid-gas interface is given by[20]

$$p=p_0+AS_0+BS_0^{3/2} \tag{16}$$

$$A=-2.3311\times10^{-3}-1.4799\times10^{-4}T_\mathrm{w}-7.520\times10^{-6}T_\mathrm{w}^2-5.5185\times10^{-8}T_\mathrm{w}^3$$

$$B=-1.1320\times10^{-5}-8.7086\times10^{-6}T_\mathrm{w}+7.4936\times10^{-7}T_\mathrm{w}^2-2.6327\times10^{-8}T_\mathrm{w}^3$$

where S_0 represents the seawater practical salinity. For inlet feed, S_0 equals 35, and S_0 at different locations along the column could be calculated based on mass conservation.

2.3 Heat transfer coefficient

The heat transfer coefficient (K) from the humid air at the shell side to the liquid film at the tube side can be expressed as follows:

$$\frac{1}{K}=\frac{\delta_\mathrm{e}}{k_\mathrm{e}}+\frac{1}{h_\mathrm{e}}+\frac{\delta_\mathrm{wall}}{k_\mathrm{wall}}+\frac{\delta_\mathrm{d}}{k_\mathrm{d}}+\frac{1}{h_\mathrm{d}} \tag{17}$$

where h_e refers to the convective heat transfer coefficient between the tube's inner surface and the saline liquid film. Eq.(18) is used to calculate h_e when the liquid film Reynolds number (Re_film) is below 2100, and Eq.(19) is used when Re_film is above 2100[19].

$$h_\mathrm{e}=0.50\times\left(\frac{k^2\rho^{4/3}C_pg^{2/3}}{\mathrm{d}Z\cdot\mu^{1/3}}\right)^{1/3}Re_\mathrm{film}^{1/9} \tag{18}$$

$$h_\mathrm{e}=0.01\times\left(\frac{k^3\rho^2g}{\mu^2}\right)^{1/3}Pr^{1/3}Re_\mathrm{film}^{1/3} \tag{19}$$

To the best of our knowledge, little literature is available on h_d, the condensation coefficient at the shell side, where more than half of the vapor-gas mixture is the non-condensable air. Zhu *et al*.[21] have studied this special process and defined h_d by

$$h_\mathrm{d}=0.0342\times\frac{\lambda_\mathrm{mix}}{d_\mathrm{e}}\frac{m_2}{C_{p,\mathrm{air}}}Re^{0.774} \tag{20}$$

$1/h_\mathrm{d}$ is one or two orders of magnitude more than the other items in Eq.(17) because of the high fractional noncondensable gas, so it is the major portion of the overall thermal resistance. In this study, convective thermal resistances ($1/h_\mathrm{e}$ and $1/h_\mathrm{d}$) and the wall thermal resistance ($\delta_\mathrm{wall}/k_\mathrm{wall}$) need to be studied and liquid-film resistances ($\delta_\mathrm{e}/k_\mathrm{e}$ and $\delta_\mathrm{d}/k_\mathrm{d}$) can be overlooked, so Eq.(17) is rewritten as follows:

$$\frac{1}{K}=\frac{1}{h_\mathrm{e}}+\frac{\delta_\mathrm{wall}}{k_\mathrm{wall}}+\frac{1}{h_\mathrm{d}} \tag{21}$$

From the experimental data, it is found that the heat loss coefficient, K_Loss, is mainly equivalent to $0.1\times K$ under the conditions of thermal insulation. On the basis of T_e, T_w, T_d, L, and F, all variables ($C_{p,\mathrm{air}}$, D_AB, λ_mix, W, H, *etc*.) can be calculated. At the top of the column, the following expression can be derived:

$$H_\mathrm{d}=H_\mathrm{e}+\frac{S}{G} \tag{22}$$

where S is the external steam flow rate. Then, such a thermally coupled HD process has been sufficiently described by Eq.(8) to (12) which can be solved using the Runge-Kutta method.

3 EXPERIMENTAL

The experimental HD column consists of 61 vertical bundled tubes enveloped in an outer shell with

inside diameter of 150mm. These heat transfer tubes are made from polypropylene filled with graphite (CFP). The length, wall thickness and outside diameter of each tube are 2m, 0.5mm, and 10mm, respectively. The thermal conductivity of CFP is 3.02W·m^{-1}·℃$^{-1}$, nearly eight times higher than that of pure polypropylene (PP, 0.35W·m^{-1}·℃$^{-1}$). The water contact angle of CFP (measured by a contact angle meter, JY-82, made in Chengde, China) is reduced from 90º to 49º after being treated by ozone. Nine segmental baffle plates are arranged in the shell side at an interval of 200mm. The total effective heat transfer area of this column is about 3.83m^2.

Figure 3 shows the experimental flow diagram. Similar to the Previous Work[15], the feed water and the carrier gas are driven by a pump and a blower, respectively. An electric boiler controlled by a temperature indicating controller is used to preheat the feed water. The external steam (atmospheric pressure, 100℃) is generated by an electric steam generator. The data for gas and feed water flow rates are measured by two rotameters. The temperatures of water and gas are measured by six thermal resistances (Pt100). A measuring cylinder is used to record the production of the condensate water. The external steam flow rate is recorded by an electronic balance (Sartorius, BL12) under the steam generator.

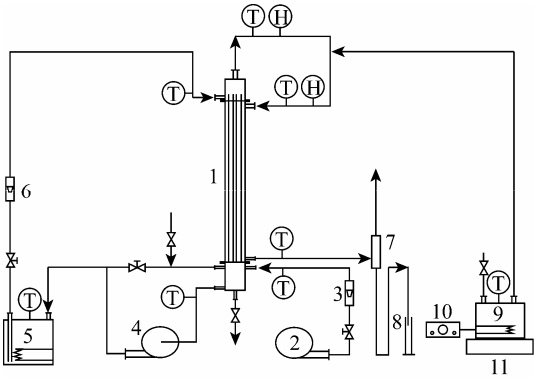

Figure 3 Schematic diagram of experimental set-up
1—CFP desalination column; 2—wind blower;
3—gas flow meter; 4—water recycling pump;
5—water heating tank; 6—liquid flow meter;
7—gas/liquid separator; 8—measuring cylinder;
9—steam generator; 10—voltage regulator;
11—electronic balance; T—thermal resistance;
H—humidity sensor

According to Bassem's study[14], the minimum gamma (mass of liquid flow, per time per width of flow, needs to entirely wet the heat transfer wall) is about 0.005kg·m^{-1}·s^{-1} on a vertical PP surface. As the surface wettability of CFP is better than that of PP (whose water contact angle is about 85°), it can be deduced that this minimum gamma value is also adequate to ensure that the inner tube walls of the present CFP column would be entirely wetted, and then a minimum feed water flow rate (multiplying minimum gamma by total inner perimeters of the tubes) of 30kg·h^{-1} can be calculated.

In this article, productivity is characterized by the fresh water obtained per hour per unit heat transfer area. The thermal efficiency is roughly evaluated by the gained output ratio (GOR), which is defined here as the flow rate ratio of the fresh water to the external steam. This definition of GOR, similar to that of Hamieh *et al*.[13], is used to evaluate the thermal efficiency of the HD unit itself. As for the thermal efficiency of the whole system, it should be evaluated after the implementation of due heat recovery measures, which are not discussed in this article.

4 RESULTS AND DISCUSSION

The effects of operating parameters, including external steam flow rate (S, kg·h^{-1}), inlet water temperature ($T_{w,in}$, ℃), water flow rate (L, kg·h^{-1}), and carrier gas flow rate (G, kg·h^{-1}), on the productivity and GOR are studied both theoretically and experimentally. At the same time, the validity of the present model is also examined by comparing the theoretical productivity and GOR with the experimental results. Because there are nine baffles at the shell side, the Reynolds number in Eq.(20) is based on the density, the viscosity, and the minimum fluid velocity of the humid air occurring at the maximum free flow area available[19].

4.1 Effect of external steam flow rate

Because of mass transfer resistance, the humid air at the top of the column is always cooler than the feed water. When the humid air enters the shell side without adding external steam, its temperature is lower than that of the tube-side feed liquid-film, so the vapor cannot be condensed immediately. Being blown by the carrier air, the temperature of the feed liquid-film at the tube side is still falling along the tubes, and thus the shell-side condensation will occur once the feed liquid-film temperature falls enough to ensure that a positive temperature difference from the shell side to the tube side is created.

The role of external steam is demonstrated by Figs.4 and 5. Here, the abnormal noncondensation portion, such as the top 0.7m of the column shown in Fig.4(a), is defined as the entrance-blank-zone (EBZ). EBZ obstructs the performance severely, and a simple solution is to add external steam. Just as shown in Fig.4(b), EBZ is shortened to 0.25m when S is raised to 0.3kg·h^{-1}. The external steam also lowers the content of noncondensable gas (air in the gas-vapor mixture, shown in Fig.4), and increases the humidity and temperature of shell-side carrier air, and then the Reynolds number, as shown in Fig.5. The more the external steam added, the shorter the EBZ is, and the bigger the temperature difference across the tube wall established. Thus higher productivity is obtained, but the GOR obtained is lower for the quantity of energy consumed, as shown in Fig.6. Considering both the productivity and the GOR, a steam flow rate of about 0.18kg·h^{-1} seems to be appropriate for the present column.

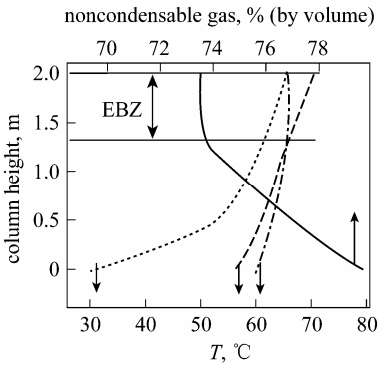

(a) S=0.08kg·h^{-1}

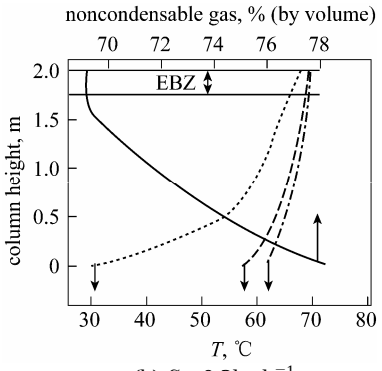

(b) S=0.3kg·h^{-1}

Figure 4 Effect of external steam flow rate on the entrance blank zone (theoretical study)
($T_{w,in}$=70℃, L=58.8kg·h^{-1}, G=8kg·h^{-1})
----- profile of T_e; – – – profile of T_w; – · – profile of T_d; —— profile of shell-side air content

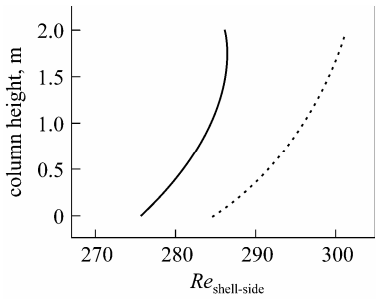

Figure 5 Effect of external steam flow rate on the profiles of shell-side *Re* (theoretical study)
($T_{w,in}$=70℃, L=58.8kg·h^{-1}, G=8kg·h^{-1})
—— shell-side *Re* with S of 0.08kg·h^{-1};
----- shell-side *Re* with S of 0.3kg·h^{-1}

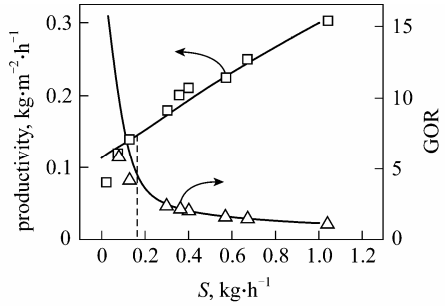

Figure 6 Effect of external steam flow rate on productivity and GOR
($T_{w,in}$=70℃, L=58.8kg·h^{-1}, G=8kg·h^{-1})
□ experimental productivity; △ experimental GOR;
—— the corresponding theoretical results

4.2 Effect of water inlet temperature

The energy for the whole HD process mainly comes from the sensible heat of feed water. The higher the temperature of feed water is (usually preferred in the range of 70—95℃)[1], the more the energy included is, and so productivity and GOR obtained are higher, just as shown in Fig.7.

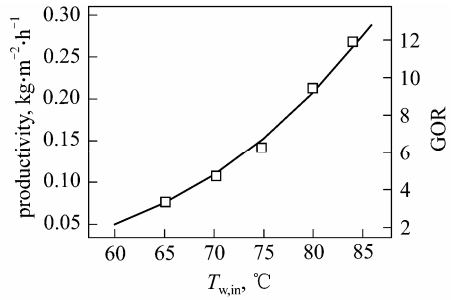

Figure 7 Effect of water inlet temperature on productivity and GOR
(L=60kg·h^{-1}, G=7.8kg·h^{-1}, S=0.08·kg·h^{-1})
□ experimental results; —— theoretical results

4.3 Effect of water flow rate

Figure 8 shows that the effects of feed water flow rate on productivity and GOR are somewhat complex. On the one hand, too little feed liquid carries too little sensible heat, which results in a low humidification efficiency, and then low humidity and temperature carrier air would subsequently cause low productivity. On the other hand, the increasing feed water flow rate decelerates its temperature-drop along the tubes and increases its mean temperature, which is disadvantageous for maintaining a temperature difference (T_d—T_w) so that the heat transfer driving force is weakened. The mean temperature difference declines from 1.7℃ to 0.9℃ when feed water flow rate increases from 20kg·h^{-1} to 60kg·h^{-1}, as shown in Fig.9. Hence, too much feed water would also reduce the productivity. Such an interaction effect makes an optimum feed water flow rate around 60kg·h^{-1}.

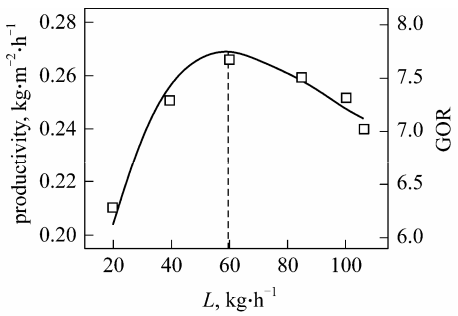

Figure 8 Effect of feed water flow rate on productivity and GOR
($T_{w,in}$=85℃, G=4.0kg·h^{-1}, S=0.13·kg·h^{-1})
□ experimental results; —— theoretical results)

4.4 Effect of carrier gas flow rate

The effect of carrier gas flow rate on productivity and GOR is also illustrated as a peak shape of the curve in Fig.10, and the optimum flow rate is about 10kg·h^{-1}.

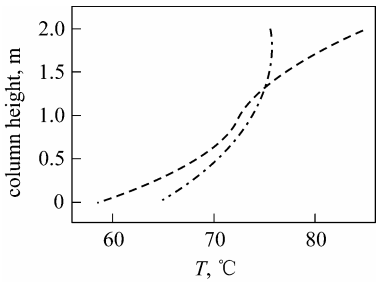

(a) L=20kg·h^{-1}

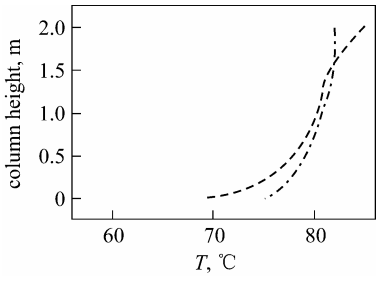

(b) L=60kg·h^{-1}

Figure 9 Effect of feed water flow rate on profiles of $T_{w,in}$ and T_d (theoretical study)
($T_{w,in}$=85℃, G=4.0kg·h^{-1}, S=0.13kg·h^{-1})
– – – profile of T_w; – · – profile of T_d

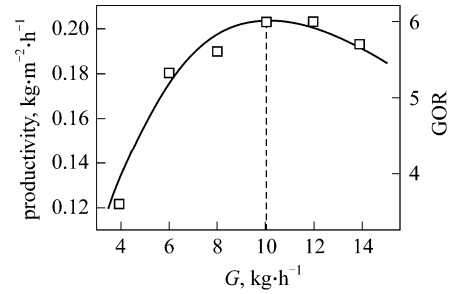

Figure 10 Effect of carrier gas flow rate on productivity and GOR
($T_{w,in}$=77℃, L=40kg·h^{-1}, S=0.13kg·h^{-1})
□ experimental results; —— theoretical results

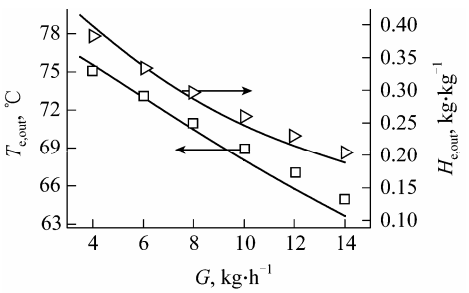

Figure 11 Effect of carrier gas flow rate on $T_{e,out}$ and $H_{e,out}$
($T_{w,in}$=77℃, L=40kg·h^{-1}, S=0.13kg·h^{-1})
□ experimental $T_{e,out}$; ▷ experimental $H_{e,out}$
—— corresponding theoretical results

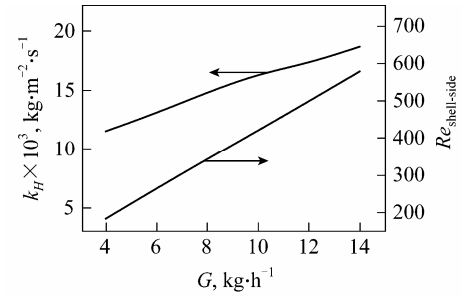

Figure 12 Effect of carrier gas flow rate on k_H and $Re_{tube-side}$ (theoretical study)
($T_{w,in}$=77℃, L=40kg·h^{-1}, S=0.13kg·h^{-1})

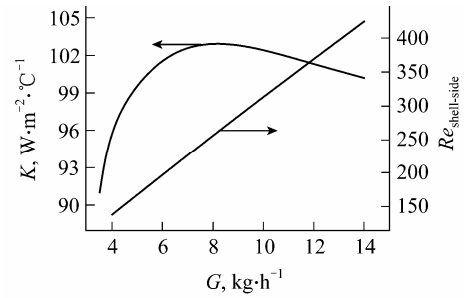

Figure 13 Effect of carrier gas flow rate on K and $Re_{shell-side}$ (theoretical study)
($T_{w,in}$=77℃, L=40kg·h^{-1}, S=0.13kg·h^{-1})

This can be explained by Figs.11, 12, and 13. On one hand, high air flow rate results in a high Reynolds number at both the tube side and the shell side, which is favorable for the tube-side mass transfer and the overall heat transfer (in Figs.12 and 13).

On the other hand, the rise in the airflow rate increases the air velocity and shortens the residence time of carrier air in the tube side. From Eq.(14) or (15), it can be seen that the increment of the mass transfer rate (k_c) cannot keep up with that of the air velocity (u), which is reflected in the tube-side Reynolds number ($Re=d\rho u/\mu$). Thus, higher airflow rate will actually weaken the humidification effect, and then decrease the temperature and humidity of air rising out of the tube ($T_{e,out}$ and $H_{e,out}$, shown in Fig.11), which are disadvantages for condensation at the shell side. As a result, when the airflow rate is too high, the heat transfer coefficient will fall (in Fig.13), and then so do the productivity and GOR.

4.5 Overall analysis

A comprehensive comparison between the columns made from CFP and copper tubes is given in Table 1.

This CFP column can reach higher productivity than that of the copper column, which shows the feasibility of applying the CFP column to the HD desalination process. However, more air and feed water are consumed in the CFP column because of the lower surface wettability (higher contact angle, θ) of the CFP tubes, which can be partially solved by recycling the air and the saline water. In conclusion, the wetting property of the inner tube wall and an efficient heat/mass recycling system will be the key problems to be solved in the further development of the process.

Table 1 Comparison between CFP and copper columns

	θ, (°)	k, $W\cdot m^{-1}\cdot℃^{-1}$	A, m^2	G, $kg\cdot h^{-1}$	L, $kg\cdot h^{-1}$	$T_{w,in}$, ℃	S, $kg\cdot h^{-1}$	Productivity, $kg\cdot m^{-2}\cdot h^{-1}$	GOR
CFP column	49	3.02	3.83	8—12	40—80	70—90	0.1—0.3	0.10—0.37	2.5—12
copper column[15]	15①	385	9.6	4—7	10—30	70—90	0.1—0.3	0.05—0.20	3—12

Note: The external steam remains at atmospheric pressure, 100℃. θ is water contact angle on the surfaces of heat transfer tubes, and A is heat transfer area.
① measured by author.

5 CONCLUSIONS

(1) On the basis of the heat/mass transfer model and the laboratory study, the studies on the thermally coupled HD desalination process using a carbon-filled plastic shell-tube column are carried out both theoretically and experimentally.

(2) The effects of several operating parameters on the performance of the column are investigated. The results show that the feed water temperature has a positive effect on the productivity and GOR, and the flow rates of external steam, feed water, and carrier air are optimized to be 0.18, 60, and 10$kg\cdot h^{-1}$, respectively.

(3) Comparing the production and GOR with a precious coppery column, this study also proves the feasibility of applying this carbon-filled plastic as heat transfer material to the HD desalination process.

NOMENCLATURE

A	area of heat transfer surface, m^2
A_H	liquid-gas interface area of mass transfer, m^2
A_{Loss}	heat loss area, which equates the inner surface area of the shell, m^2
C_p	heat capacity at constant pressure, $J\cdot kg^{-1}\cdot℃^{-1}$
$C_{p,air}$	heat capacity of humid air, at constant pressure, $J\cdot kg^{-1}\cdot℃^{-1}$
D_{AB}	diffusion coefficient of water vapor in air, $m^2\cdot s^{-1}$
d	tube's inside diameter, m
d_e	equivalent diameter, m
F	fresh water flow rate, $kg\cdot h^{-1}$
G	carrier gas flow rate, $kg\cdot h^{-1}$
g	acceleration due to gravity, $m\cdot s^{-2}$
H	humidity (vapor/air), $kg\cdot kg^{-1}$
H_w	humidity of air at the water-air interface, $kg\cdot kg^{-1}$
h	film coefficient, $W\cdot m^{-2}\cdot℃^{-1}$
K	heat transfer coefficient, $W\cdot m^{-2}\cdot℃^{-1}$
k	thermal conductivity, $W\cdot m^{-1}\cdot℃^{-1}$
k_c	gas phase mass transfer coefficient, $m\cdot s^{-1}$
k_H	tube-side mass transfer coefficient, $kg\cdot m^{-2}\cdot s^{-1}$
L	water flow rate at humidification side, $kg\cdot h^{-1}$
M	molecular weight, $kg\cdot kmol^{-1}$
m	intermediate variable, (m_1, m_2: $kJ\cdot kg^{-1}\cdot℃^{-1}$; m_3, m_4: $kg\cdot kg^{-1}\cdot℃^{-1}$)
n	structural parameter, m
P	gas phase total pressure, Pa
Pr	Prandtl number
p	saturated vapor pressure of sea water, Pa (mmHg)
p_{BM}	air partial pressure difference, Pa
p_0	saturated vapor pressure of pure water, Pa(mmHg)
Q	quantity of heat, W
R	universal gas constant (=$8.314J\cdot mol^{-1}\cdot K^{-1}$)
Re	Reynolds number
S	external steam flow rate, $kg\cdot h^{-1}$
Sc	Schmidt number
Sh	Sherwood number
S_0	practical salinity
T	temperature, ℃ or K
u	velocity, $m\cdot s^{-1}$
W	enthalpy of humid air, $J\cdot kg^{-1}$
δ	thickness, m
θ	water contact angle on the surfaces of heat transfer tubes, (°)
λ_{mix}	thermal conductivity of humid air, calculated from those of vapor and air according to the ideal mixing rule, $W\cdot m^{-1}\cdot℃^{-1}$
μ	viscidity, Pa·s
ρ	density, $kg\cdot m^{-3}$

Subscripts

A	active component (water vapor)
air	air
amb	ambient
B	inert component (air)
d	shell (condensation) side
e	tube (evaporation) side
film	liquid falling film
in	inlet
Loss	loss of heat to ambient
laminar	laminar flow
out	exit
transition	transition flow
w	water
wall	tube wall

REFERENCES

1 Bourouni, K., Chaibi, M.T., Tadrist, L., "Water desalination by humidification and dehumidification of air: State of the art", *Desalination*, **137**, 167—176(2001).

2 Parekh, S., Farid, M.M., Selman, J.R., Al-Hallaj, S., "Solar desalination with a humidification-dehumidification technique —A comprehensive technical review", *Desalination*, **160**, 167—186(2004).

3 García-Rodríguez, L., "Seawater desalination driven by renewable energies: a review", *Desalination*, **143**, 103—113(2002).

4 Bourouni, K., Martin, R., Tadrist, L., Chaibi, M.T., "Heat transfer and evaporation in geothermal desalination units", *Appl. Energy*, **64**, 129—147(1999).

5 Bourouni, K., Chaibi, M.T., "Modelling of heat and mass transfer in a horizontal-tube falling-film condenser for brackish water desalination in remote areas", *Desalination*, **166**, 17—24(2004).

6 Nawayseh, N.Kh., Farid, M.M., Al-Hallaj, S., Al-Timimi, A.R., "Solar desalination based on humidification process--I. Evaluating the heat and mass transfer coefficients", *Energy Conv. Manag.*, **40**, 1423—1439(1999).

7 Dai, Y.J., Wang, R.Z., Zhang, H.F., "Parametric analysis to improve the performance of a solar desalination unit with humidification and dehumidification", *Desalination*, **142**, 107—118(2002).

8 Nafey, A.S., Fath, H.E.S., El-Helaby, S.O., Soliman, A., "Solar desalination using humidification-dehumidification processes. Part II. An experimental investigation", *Energy Conv. Manag.*, **45**, 1263—1277(2004).
9 Hashemifard, S.A., Azin, R., "New experimental aspects of the carrier gas process (CGP)", *Desalination*, **164**, 125—133(2004).
10 Al-Enezi, G., Ettouney, H., Fawzy, N., "Low temperature humidification dehumidification desalination process", *Energy Conv. Manag.*, **47**, 470—484(2006).
11 Albers, W.F., Beckman J.R., "Brackish and seawater desalination by a new carrier-gas process", In: NWSIA 1988 Conf., San Diego, CA, USA (1988).
12 Beckman, J.R., "Method and apparatus for simultaneous heat and mass transfer utilizing a carrier-gas", WO Pat., 01/07134 A1 (2001).
13 Hamieh, B.M., Beckman, J.R., Ybarra, M.D., "Brackish and seawater desalination using a 20 ft^2 dewvaporation tower", *Desalination*, **140**, 217—226(2001).
14 Bassem, M.H., "A theoretical and experimental study of seawater desalination using dewvaporation", Ph.D. Thesis, Arizona State University, USA(2001).
15 Xiong, R.H., Wang, S.C., Wang, Z., "Experimental investigation of a vertical tubular desalination unit using humidification-dehumidification process", *Chin. J. Chem. Eng.*, **13**(3), 324—328(2005).
16 Wang, S.C., Cheng, H.G., Ding, T., "Manufacturing method and apparatus for a plastic humidification-dehumidification desalination column", CN Pat., 1850634 A (2006). (in Chinese)
17 Xiong, R.H., Wang, S.C., Wang, Z., "A mathematical model for a thermally coupled humidification-dehumidification desalination process", *Desalination*, **196**, 177—187(2006).
18 Bell, A.A., Jr., HVAC Equations, Data, and Rules of Thumb, McGraw-Hill, Inc., New York, 385-391(2000).
19 Perry, R.H., Green, D.W., Perry's Chemical Engineers' Handbook, 7th ed., McGraw-Hill, Inc., New York (1997).
20 Millero, F. J., Leung, W.H., "The thermodynamics of seawater at one atmosphere", *Am. J. Sci.*, **276**, 1035—1077(1976).
21 Zhu, A.M., Wang, S.C., Sun, J.X., Xie, L.X., Wang, Z., "Effects of high fractional noncondensable gas on condensation in the dewvaporation desalination process", *Desalination*, **214**, 128—137(2007).